

We are IntechOpen, the world's leading publisher of Open Access books Built by scientists, for scientists

6,900

Open access books available

186,000

International authors and editors

200M

Downloads

Our authors are among the

154

Countries delivered to

TOP 1%

most cited scientists

12.2%

Contributors from top 500 universities



WEB OF SCIENCE™

Selection of our books indexed in the Book Citation Index
in Web of Science™ Core Collection (BKCI)

Interested in publishing with us?
Contact book.department@intechopen.com

Numbers displayed above are based on latest data collected.
For more information visit www.intechopen.com



Iterative Restoration Methods to Loose Estimations Dependency of Regularized Solutions

Miguel A. Santiago¹, Guillermo Cisneros¹ and Emiliano Bernués²

¹*Polytechnic University of Madrid, Department of Signals,
Systems and Radiocommunications*

²*University of Zaragoza, Department of Electronic Engineering and Communications
Spain*

1. Introduction

Image restoration is a classical area of digital image processing, appearing in many applications such as remote sensing, medical imaging, astronomy or computerized tomography (González & Woods, 2007). Simply put, the aim is to recover an original image which has been degraded due to the imperfections in the acquisition system: blurring and noise. Restoring this degradation leads to an ill-posed problem since the simple inverse using least-squares yields highly noise-sensitive solutions. A large number of techniques have been developed to cope with this issue, most of them under the regularization or the Bayesian frameworks (a complete review can found in Banham & Katsaggelos, 1997; Bovik, 2005; Chan & Shen, 2005).

Mathematical regularization is used to include prior knowledge about the original image in the restoration process which allows stabilizing the solution in the face of noise. However, two main problems arise for such a regularization approach. First, the non-local property of the underlying convolution implies that part of the blurred image near the boundary integrates information of the original scenery outside the field of view. However, this information is not available in the deconvolution process and may cause strong ringing artifacts on the restored image, i.e., the well-known boundary problem (Woods et al., 1985). Typical methods to counteract the boundary effect is to make assumptions about the behavior of the original image outside the field of view such as Dirichlet, Neuman, periodic or other recent conditions in Calvetti & Somersalo, 2005; Martinelli et al., 2006; Liu & Jia, 2008. Secondly, restoration methods depend on a wide set of parameters which can be roughly grouped into three categories: parameters with respect to the degradation process, the noise and the original image. All parameters require an accurate prior estimation because small errors in their values lead to important deviations in the restoration results. In fact, classical restoration methods tend to improve the estimation of those parameters without prior knowledge about the real scenery, which is known as blind deconvolution (Campisi & Egiazarian, 2007; Molina et al., 2006). The boundary problem and the sensitivity to estimations are the issues to solve in this chapter by means of two iterative algorithms.

The first algorithm copes with the boundary problem taking a blurred image defined in the field of view, but with neither any image information nor prior assumption on the boundary conditions. Furthermore, the objective is not only to reduce the ringing artifacts on the whole image, but also reconstruct the missed boundaries of the original image which becomes a significant step of the research. Neural networks are very well suited to combine both processes in the same restoration algorithm and thus we provide a solution based on a Multilayer Perceptron (MLP) in line with a backpropagation strategy. Other neural-net-based restoration techniques (Paik & Katsaggelos, 1992; Sun, 2000; Han & Wu, 2004) have been proposed in the literature with the Hopfield's model, but they are typically time-consuming and large scaled. In the light of the good results of the total variation (TV) regularizer in recent deconvolution (Wang et al., 2005; Wu et al., 2007; Bioucas-Dias et al., 2006; Oliveira et al., 2009; Molina et al., 2006), we have used it to set the minimization mechanism of the net. The proposed scheme is then an iterative method which performs repeatedly a cycle of two steps: forward and backward, simulating respectively restoration and degradation processes at each iteration.

Following the same iterative concept of restoration-degradation, we present a second algorithm in the frequency domain to reduce the dependency on the estimation of parameters. Hence, a novel desensitized restoration filter is designed by applying an iterative algorithm over the original filter. Analyzing the sensitivity properties of this filter and setting a criterion to choose the number of iterations, we come up with an expression for the desensitized algorithm for traditional filters such as Wiener and Tikhonov (González & Woods, 2007). The results of this algorithm pretend to increase the robustness of the restoration methods when estimating parameters such as the noise variance or degradation related parameters.

The chapter is organized as follows. In the next section, we provide a detailed formulation of the two restoration problems of the chapter, establishing naming conventions and the mathematical basis of the respective algorithms. In Sec. 3, we present the architecture of the iterative methods under analysis: MLP and desensitized filter, going into details about the adjustment of the synaptic weights of the net in every layer and the computation of the number of iterations for the desensitized scheme respectively. We present some experimental results in Sec. 4 and, finally, concluding remarks are given in Sec. 5.

2. Problem formulation

To start with image restoration a better understanding of the acquisition system is required. Because of physical limitations or human errors in operating imaging systems, the observed image is actually a degraded version of the original scene. For instance, deterministic degradations such as motion blurs, out of focus lens or effects of atmospheric turbulence in remote sensing cause a bandwidth reduction of the original image. In a linear acquisition scenario this distortion is mathematically described as a point spread function (PSF) denoted by $h(i, j)$, which represents a two dimensional filter mask of size $M_1 \times M_2$. For sake of simplicity we consider spatially invariant functions such that the degradation is independent of the position. In addition to blurring, noise is always present in the observed image due to stochastic variations in the process of image formation, the transmission medium or the recording system. We assume a common additive zero-mean Gaussian white

noise $n(i, j)$ of variance σ_n^2 , which also represents the quantization error coming from digitalizing images. The statistical descriptors of the noise are likewise assumed to not vary spatially.

Let $x(i, j)$ be the unknown gray-scaled original image of size $L_1 \times L_2$, degraded by a PSF $h(i, j)$ and corrupted by a noise sample $n(i, j)$. Therefore, we can express the observed image $y(i, j)$ as

$$y(i, j) = h(i, j) ** x(i, j) + n(i, j) \quad (1)$$

where $**$ represents the two dimensional convolution operator. In order to simplify expressions, we shall use lexicographic notation by stacking the columns of a matrix in a vector. Then, the equation (1) is rewritten as

$$\mathbf{y} = \mathbf{H}\mathbf{x} + \mathbf{n} \quad (2)$$

defined by the original image \mathbf{x} of length $L = L_1 \times L_2$, whereas the degraded image \mathbf{y} is a \tilde{L} sized vector bigger than the original image as result of the non-local property of the convolution operation (see 2.1). In terms of blurring, \mathbf{H} is known as the convolution matrix of size $\tilde{L} \times L$ built from the PSF and using the so-called boundary conditions that we will discuss later.

Another way to represent the equation (1) is through its spectral equivalence. By applying discrete Fourier transform (González & Woods, 2007) to that expression, we obtain

$$Y(\varpi_i, \varpi_j) = H(\varpi_i, \varpi_j)X(\varpi_i, \varpi_j) + N(\varpi_i, \varpi_j) \quad (3)$$

where (ϖ_i, ϖ_j) are the spatial frequency coordinates, and the capital letters represent Fourier transforms. In the frequency domain it is assumed that the observed image is a circular period that wraps around the edges, what it is not physically true but typically used for computational convenience.

In view of the above equations, image restoration is defined as an inverse problem that tries to estimate the original image $\hat{\mathbf{x}}$ from the observed image \mathbf{y} using the blurring model \mathbf{H} . However, a simple least-squares solution is not possible since the presence of noise or the singularity of the matrix \mathbf{H} make it an ill-conditioned problem. Thus, a regularization method is needed to control the high sensitivity to noise as explained in Banham & Katsaggelos, 1997. Quite a few examples have been presented in the literature by means of the classical Tikhonov regularization which establishes

$$\hat{\mathbf{x}} = \arg \min_{\mathbf{x}} \left\{ \frac{1}{2} \|\mathbf{y} - \mathbf{H}\mathbf{x}\|_2^2 + \frac{\lambda}{2} \|\mathbf{D}\mathbf{x}\|_2^2 \right\} \quad (4)$$

where $\|\mathbf{z}\|_2^2 = \sum_i z_i^2$ denotes the ℓ_2 norm, $\hat{\mathbf{x}}$ is the restored image and \mathbf{D} is the regularization operator, built on the basis of a high pass filter mask \mathbf{d} of size $N = N_1 \times N_2$. The first term in (4) is the ℓ_2 residual norm appearing in the least-squares approach and

ensures fidelity to data. The second term is the so-called *regularizer* which captures prior knowledge about \mathbf{x} through an additional ℓ_2 penalty term involving the image. The hyperparameter (or regularization parameter) λ is a critical value which measures the trade-off between a good fit and a regularized solution.

Alternatively, the total variation (TV) regularization proposed by Rudin et al., 1992, has become very popular in recent research as it achieves to preserve edges in the restored image. A discrete version of the TV deblurring problem is given by

$$\hat{\mathbf{x}} = \arg \min_{\mathbf{x}} \left\{ \frac{1}{2} \|\mathbf{y} - \mathbf{H}\mathbf{x}\|_2^2 + \lambda \|\nabla \mathbf{x}\|_1 \right\} \quad (5)$$

where $\|\mathbf{z}\|_1$ denotes the ℓ_1 norm (i.e., the sum of the absolute value of the elements) and ∇ stands for the discrete gradient operator. The ∇ operator is defined by the matrices \mathbf{D}^s and \mathbf{D}^v as

$$\nabla \mathbf{x} = \left| \mathbf{D}^s \mathbf{x} \right| + \left| \mathbf{D}^v \mathbf{x} \right| \quad (6)$$

built on the basis of the respective masks \mathbf{d}^s and \mathbf{d}^v of size $N = N_1 \times N_2$, which turn out the horizontal and vertical first order differences of the image. Compared to the expression (4), the TV regularization provides a ℓ_1 penalty term which can be thought as a measure of signal variability. Once again, λ is the critical regularization parameter to control the weight assigned to the regularizer with respect to the data misfit term.

Significant amount of work has been addressed to solve any of the above regularizations and mainly the TV deblurring in recent times (Chan & Shen, 2005). However, there are two important issues in those algorithms which require making assumptions and constraining the regularized solution: boundary conditions and parameters estimations. This chapter provides two novel iterative methods aimed to loose this dependency and achieve a more robust solution in terms of estimations. Let us analyze each problem separately.

2.1 Boundary conditions

As defined in González & Woods, 2007, the convolution operator of equation (1) integrates a portion of the original scenery \mathbf{x} into a single point by weighting the nearby pixels by a 180 degrees rotated mask \mathbf{h} . When computing the pixels near the boundary and depending on the size of the PSF, many pixels of \mathbf{y} contain information coming from the original scenery outside the field of view (FOV) which is indeterminate. We refer to this phenomenon and to its consequences as *boundary effect*. It is well known that if the boundary effect is not properly taken into account, it may cause strong ringing artifacts on the deconvolved image. For that reason, various methods of the literature try to counteract this effect by selecting appropriate boundaries conditions (BCs). These boundary conditions are included in the model of \mathbf{H} used in deconvolution as

$$\mathbf{H} = \mathbf{T} + \mathbf{B} \quad (7)$$

where \mathbf{T} has a Toeplitz structure and \mathbf{B} is often structured, sparse and low rank, and specifically defined for every BC. Common cases are the *Zero* (Bertero & Bocacci, 1998), *Periodic* (Bertero & Bocacci, 1998), *Reflective* (Ng et al., 1999) or *Anti-reflective* (Martinelly et al., 2006) boundary conditions.

As a result of the convolution, it can be easily demonstrated (see Fig. 1) that the degraded image \mathbf{y} increases its size with respect to the original image \mathbf{x} from L to \tilde{L} as

$$\tilde{L} = (L_1 + 2B_1) \times (L_2 + 2B_2) \tag{8}$$

where B_1 and B_2 are the respective horizontal and vertical bandwidths of the PSF, then the length of \mathbf{h} is $M = M_1 \times M_2 = (2B_1 + 1) \times (2B_2 + 1)$. We have gray colored the pixels affected by the boundary conditions which are not actually present in a real observation. Therefore, a real observed image \mathbf{y}_{real} is a truncated version of the convolution process to the region called field of view

$$FOV = [(L_1 - 2B_1) \times (L_2 - 2B_2)] \subset \tilde{L} \tag{9}$$

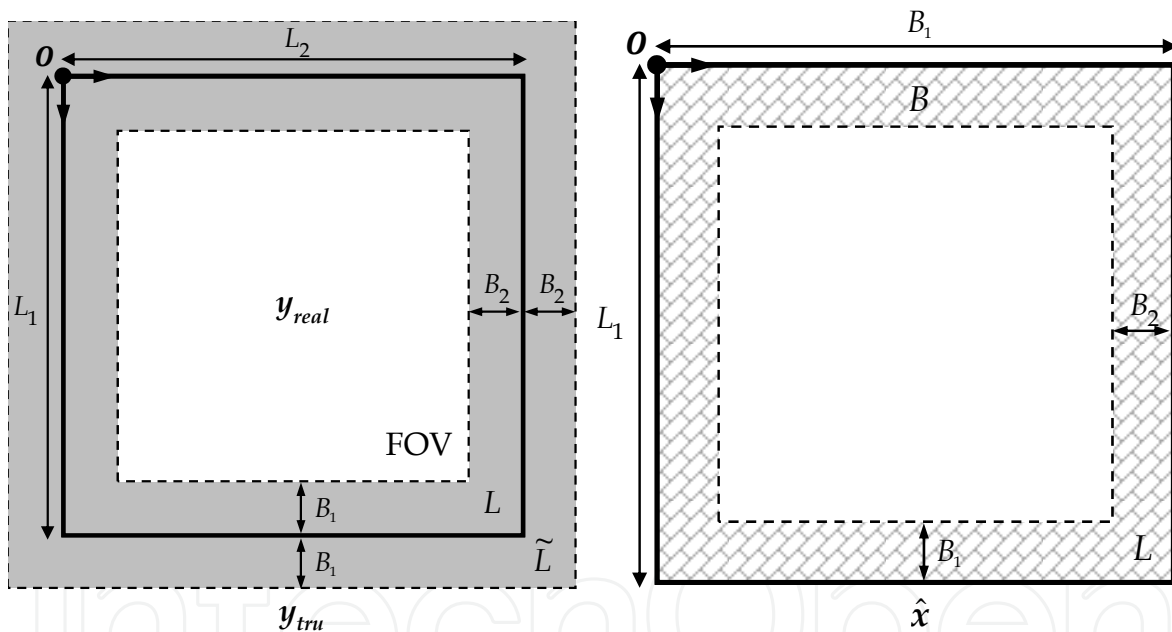


Fig. 1. Real observed image defined in the field of view (left). Restored image which indicates the boundary reconstruction area (right).

Common deblurring methods deal with this real image \mathbf{y}_{real} and try to restore it minimizing the boundary ringing as much as possible using BCs on the model \mathbf{H} like (7). However, the restored image is only obtained within the FOV domain, that is smaller than the original image size L . Our goal is to not only improve the restoration on the whole image but also reconstruct the boundaries that are missed in the observation, without neither any image information nor prior assumption on the boundary conditions.

Let us define an image \mathbf{y}_{tru} which represents this observed image \mathbf{y}_{real} using a $\text{trunc}\{\cdot\}$ operator that removes (zero-fixes) the pixels of the boundary region, that is to say

$$y_{tru}(i, j) = \text{trunc}\left\{\mathbf{H}_a \mathbf{x} + \mathbf{n}\right\}_{(i,j)} = \begin{cases} \mathbf{y}_{real} = \mathbf{H}_a \mathbf{x} + \mathbf{n}_{(i,j)} & \forall (i, j) \in \text{FOV} \\ 0 & \text{otherwise} \end{cases} \quad (10)$$

where \mathbf{H}_a denotes the Toeplitz matrix when not using boundary conditions (aperiodic model). Therefore, we aim to restore this truncated image \mathbf{y}_{tru} in spite of the discontinuity at the boundaries and reconstruct the region B depicted in Fig. 1

$$B = L - \text{FOV} \quad (11)$$

whose area is calculated by $B = (L_1 - B_1) \times 4B_1$, if we consider square dimensions such that $B_1 = B_2$ and $L_1 = L_2$.

Particular, we intend to study an iterative algorithm using the TV regularizer which loose the dependency on the boundary conditions. So we redefine the restoration problem (5) including the $\text{trunc}\{\cdot\}$ operator as

$$\hat{\mathbf{x}} = \arg \min_{\mathbf{x}} \left\{ \frac{1}{2} \|\mathbf{y} - \text{trunc}\{\mathbf{H}_a \mathbf{x}\}\|_2^2 + \lambda \left\| \text{trunc}\left\{ \left| \mathbf{D}_a^s \mathbf{x} \right| + \left| \mathbf{D}_a^h \mathbf{x} \right| \right\} \right\|_1 \right\} \quad (12)$$

where the subscript \mathbf{a} denotes the aperiodic formulation of every matrix operator. An equivalent analysis for the Tikhonov regularizer can be found in Santiago et al., 2010.

2.2 Estimations dependency

If we have a look to any restoration method of the literature, we come up with their dependency on a wide set of parameters which must be estimated a priori. We can group them basically into three classes

- Parameters with respect to the blurring process.
- Parameters with respect to the noise.
- Parameters with respect to the original image.

In terms of blurring, the convolution matrix \mathbf{H} is not always available in the restoration process and thus it is required to make assumptions about its parameters, such as the length of motion or the radius of out-of-focus among others. We can find a lot of articles devoted to estimate the PSF which are normally referred to as blind deconvolution. Regarding noise we have assumed a Gaussian white noise from the very beginning, so the concrete parameter is just the variance σ_n^2 . Finally, the parameters related to the original image have to do with the regularization term of the equations (4) or (5) and, in turn, with the regularization parameter λ .

Blind deconvolution methods try to obtain the more accurate parameters but deal with a problem known as sensitivity to estimations, that is to say, relatively small deviations from the real (unknown) values have a severe impact on the restoration quality. Therefore, we aim to define an algorithm that improves the results of a restoration scheme when having wrong estimates of the said parameters, namely, a desensitization process.

We shall work in the frequency domain for this issue so we take for granted the circular boundary conditions of the previous section. In particular, our goal is to desensitize two

common algorithms of the literature defined in the Fourier space: Wiener and Tikhonov (Bovik, 2005). Both methods are completely linear so described by a restoration filter as

$$\hat{X}(\varpi_i, \varpi_j) = G(\varpi_i, \varpi_j)Y(\varpi_i, \varpi_j) \quad (13)$$

where $G(\varpi_i, \varpi_j)$ denotes the Fourier transform of the restoration filter. In order to simplify notation, the reference to the element (ϖ_i, ϖ_j) of the matrices in the frequency domain will be removed from all formulae throughout the remainder of the chapter. They are differentiated from the variables of the boundary problem because those are in bold. Besides, it must be taken into account that all mathematical expressions involving matrices in the Fourier Transform domain are scalar computations for each frequency component (ϖ_i, ϖ_j) .

From González & Woods, 2007, it is demonstrated that

- Wiener Filter

$$G = \frac{H^*}{|H|^2 + \frac{S_{nn}}{S_{xx}}} \quad (14)$$

where H^* represents the complex conjugate of H , S_{xx} and S_{nn} are the respective spectral densities of the original image \mathbf{x} and the noise \mathbf{n} .

- Tikhonov Filter

$$G = \frac{H^*}{|H|^2 + \lambda|D|^2} \quad (15)$$

where D is the Fourier transform of the regularization operator \mathbf{D} in (4).

Let us symbolize the restoration filter as \hat{G} when calculated by estimations (not real values) as well as the rest of variables involved in (14) and (15) such as \hat{H} , \hat{S}_{xx} , \hat{S}_{yy} and $\hat{\lambda}$. Therefore, we shall define an iterative method which achieves a filter G' based on the original \hat{G} with less sensitivity to wrong estimations.

3. Iterative methods

In this section we propose two algorithms to cope with the aforementioned constraints of a restoration problem: boundary conditions and estimation dependency. Both methods are iterative and lead to various restoration-degradation processes repeated a certain number of times. A detailed analysis is devoted to each algorithm in the following sections.

3.1 MLP approach

The main issues addressed by this algorithm are

- Restore a real observed image \mathbf{y}_{real} without neither any image information nor prior assumption on the boundary conditions.

- Remove boundary ringing in spite of the discontinuity at the boundaries.
- Reconstruct the boundary region B so that the restored image has the same size L as the original image.
- Make use of the TV regularizer.

To go around this problem we know that neural networks are particularly well-suited as their ability to nonlinear mapping and self-adaptiveness. In fact, the Hopfield network has been used in the literature to solve the optimization problem (4) and recently some neural network solutions as in Wang, 2005 and Wu, 2007 deal with the TV regularization (5).

Our proposal is a MLP (Multiplayer Perceptron) with back-propagation as illustrated in Fig. 2. The input layer of the net consists of \tilde{L} neurons with inputs $y_1, y_2, \dots, y_{\tilde{L}}$ being respectively the \tilde{L} pixels of the truncated image \mathbf{y}_{tru} . At any generic iteration m , the output layer is defined by L neurons whose outputs $\hat{x}_1(m), \hat{x}_2(m), \dots, \hat{x}_L(m)$ are respectively the L pixels of an approach $\hat{\mathbf{x}}(m)$ to the restored image. After \bar{m} iterations, the neural net outcomes the actual restored image $\hat{\mathbf{x}} = \hat{\mathbf{x}}(\bar{m})$. On the other hand, the hidden layer consists of only two neurons, although being enough to achieve good restoration results while keeping low complexity of the network.

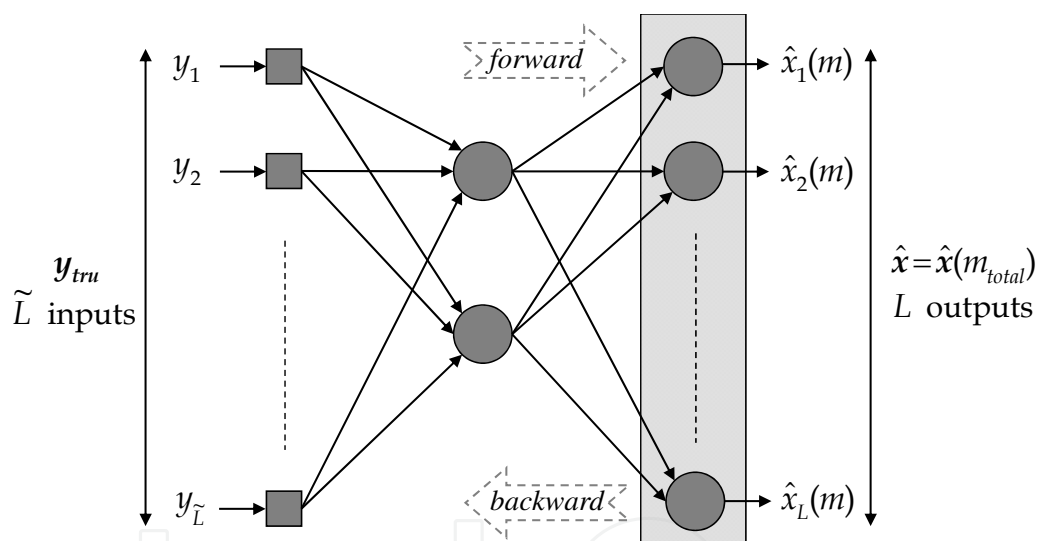


Fig. 2. MLP scheme adopted for image restoration.

The neural network undertakes two processes iteratively: forward and backward. The former is the result of applying from left to right the equations of every layer. It is actually the restoration step. The latter is the back-propagation process where the network must minimize a regularized error function which we will set to the expression (12). It means to adjust the synaptic coefficients of every single neuron from right to left and can be thought as a reblurring step. Since the $\text{trunc}\{\cdot\}$ operator is involved in all those expressions, the truncation of the boundaries is performed at every iteration but also their reconstruction as indicated by the L size at the output. What deserves attention is that no a priori knowledge, assumption or estimation concerning the unknown borders is needed to perform the regeneration. Generally speaking it could be explained by the neural net nature which is able to learn about the degradation model.

A restored image is therefore obtained in real conditions on the basis of a global energy minimization strategy, with reconstructed borders while adapting the center of the image to the optimum solution and thus making the ringing artifact negligible. Finally, we recall that the input to the net is always the image \mathbf{y}_{tru} as no net training is required.

3.1.1 Adjustment of the neural net

Let us define each layer of Fig. 2 as an input vector \mathbf{p} of size $R \times 1$, a synaptic weight matrix \mathbf{W} of $S \times R$ in size, and a $S \times 1$ output vector \mathbf{z} of the layer. We utilize a log-sigmoid expression for the transfer function $\varphi\{\cdot\}$ and a null bias vector. A superscript is used to denote the number of layer, but it will be removed when deduced by context. So we can redraw our MLP as depicted in Fig. 3 where we have symbolized the variation of the synaptic matrixes of every layer.

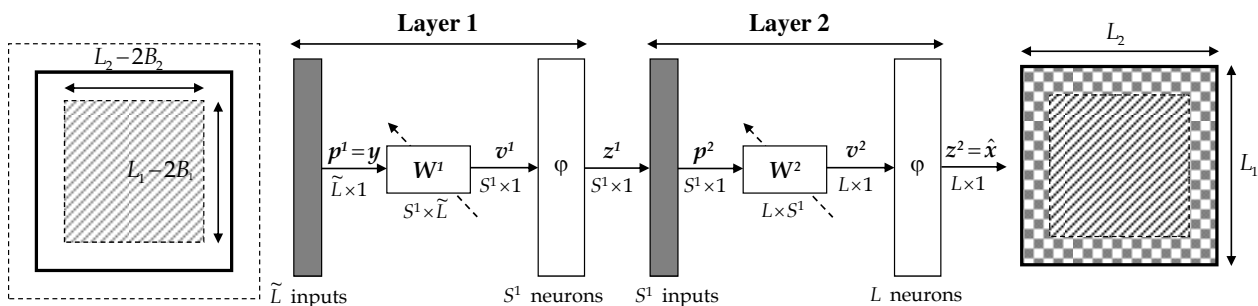


Fig. 3. MLP algorithm with matrix-vector notation.

A variant of the well-known algorithm of back-propagation is used to adjust those matrixes with the truncated cost function of (12). Let $\Delta \mathbf{W}^i(m+1)$ be the correction applied to the weight matrix \mathbf{W}^i of the layer i at the $(m+1)^{th}$ iteration. Then,

$$\Delta \mathbf{W}^i(m+1) = -\eta \frac{\partial E(m)}{\partial \mathbf{W}^i(m)} \tag{16}$$

where $E(m)$ stands for the cost error function after m iterations at the output of the net and the constant η indicates the learning speed. Defining the vectors $\mathbf{e}(m)$ and $\mathbf{r}(m)$ for the respective error and regularization terms at the output layer after m iterations

$$\mathbf{e}(m) = \mathbf{y} - \text{trunc}\{\mathbf{H}_a \hat{\mathbf{x}}(m)\} \tag{17}$$

$$\mathbf{r}(m) = \text{trunc}\left\{\left|\mathbf{D}_a^s \hat{\mathbf{x}}(m)\right| + \left|\mathbf{D}_a^r \hat{\mathbf{x}}(m)\right|\right\} \tag{18}$$

we can rewrite the restoration error from (12)

$$E(m) = \frac{1}{2} \|\mathbf{e}(m)\|_2^2 + \lambda \|\mathbf{r}(m)\|_1 \tag{19}$$

Now we aim to compute the so-called gradient matrix $\frac{\partial E(m)}{\partial \mathbf{W}^i(m)}$ in the layers of the MLP. A

high detailed analysis can be found in Santiago et al., 2010 based on the algorithm of majorization-minimization developed by Bioucas-Dias et al., 2006 when facing a TV regularization problem like (5). Let us summarize the main results below:

$$\Delta \mathbf{W}^i(m+1) = -\eta \boldsymbol{\delta}^i(m) (\mathbf{z}^{i-1}(m))^T \quad (20)$$

where $\boldsymbol{\delta}(m)$ stands for the local gradient vector and is defined for a MLP of J layers as:

- Output layer ($i = J$)

$$\boldsymbol{\delta}(m) = \varphi\{\mathbf{v}(m)\} \circ (-\mathbf{H}_a^T \mathbf{e}(m) + \lambda \mathbf{D}_a^T \boldsymbol{\Omega}(m) \mathbf{r}(m)) \quad (21)$$

where \circ denotes the Hadamard (elementwise) product, \mathbf{D}_a is a composition of the matrices

\mathbf{D}_a^ξ and \mathbf{D}_a^μ as $\mathbf{D}_a = \left[(\mathbf{D}_a^\xi)^T \ (\mathbf{D}_a^\mu)^T \right]^T$ and $\boldsymbol{\Omega}(m)$ represents a weigh matrix which controls the influence of regions with high intensity variation

$$\boldsymbol{\Omega}(m) = \begin{bmatrix} \boldsymbol{\Lambda}(m) & 0 \\ 0 & \boldsymbol{\Lambda}(m) \end{bmatrix} \quad (22)$$

$$\text{with } \boldsymbol{\Lambda}(m) = \text{diag} \left(\frac{1}{2\sqrt{(\mathbf{D}_a^\xi \hat{\mathbf{x}}(m))^2 + (\mathbf{D}_a^\mu \hat{\mathbf{x}}(m))^2 + \varepsilon}} \right)$$

- Any hidden layer ($i < J$)

$$\boldsymbol{\delta}^i(m) = \text{diag} \left(\varphi\{\mathbf{v}^i(m)\} \right) (\mathbf{W}^{i+1}(m))^T \boldsymbol{\delta}^{i+1}(m) \quad (23)$$

3.1.2 Algorithm parameters

Due to the iterative nature of the algorithm the first parameter to establish has to do with the stop rule. It is a condition such that either the number of iterations is more than a maximum; or the error $E(m)$ converges and, thus, the error change $\Delta E(m)$ is less than a threshold; or, even, this error $E(m)$ starts to increase. If one of these conditions comes true, the algorithm concludes and the final outgoing image is the restored image $\hat{\mathbf{x}} = \hat{\mathbf{x}}(\bar{m})$.

In the image restoration field it is remarked the importance of the parameter λ . Low values of λ yield oscillatory solutions because of the presence of noise or discontinuities; high values of λ yield over smoothed results though. For that reason, the literature has given significant attention to it with popular approaches such as the unbiased predictive risk estimator (UPRE), the generalized cross validation (GCV), or the L-curve method; see Vogel, 2002 for an overview and references. Most of them were particularized for a Tikhonov

regularizer, but lately researches aim to provide solutions for the TV regularization. Specifically, the Bayesian framework leads to successful approaches in this respect.

In Santiago et al., 2010 we adjusted λ with solutions coming from the Bayesian state-of-art. However, we still need to investigate a particular algorithm for the MLP since those Bayesian approaches work only for circulant degradation models, but not for the truncated image of this chapter. So we shall compute yet a hand-tuned λ which optimizes the results.

As for learning speed it was already demonstrated that η shows lower sensitivity compared to λ . In fact, its main purpose is to speed up or slow down the convergence of the algorithm. Then, for the sake of simplicity, we shall assume $\eta = 2$ for the images of 256×256 in size.

3.2 Desensitization approach

The second of our methods go around the following issues

- Desensitize the restoration filter (assumed linear) with respect to wrong parameter estimations.
- Counteract the effects of mistaking parameters in order to achieve a better restoration quality compared to that without desensitization.
- Alternative to classic restoration approaches which focus on obtaining accurate estimations.
- Particularization to Wiener and Tikhonov filters

Let us define an expression for the desensitized filter G' based on the original \hat{G} in the frequency domain. Again our approach is an iterative algorithm as illustrated in Fig. 4.

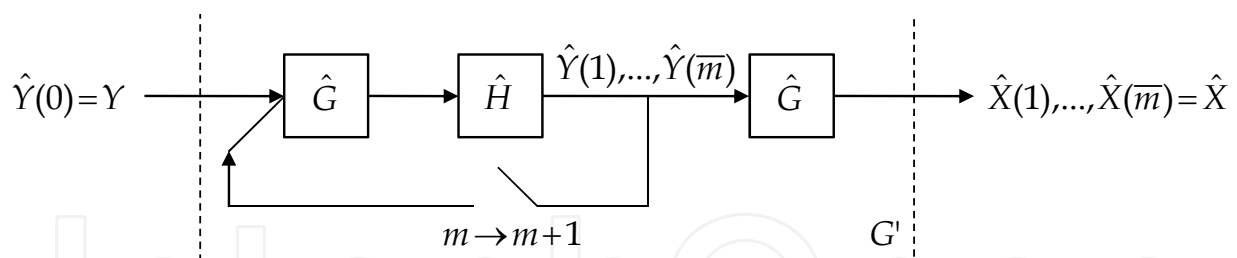


Fig. 4. Desensitized restoration scheme.

The input at any iteration m ($m = 1, 2, \dots, \bar{m}$) is an image $\hat{Y}(m)$ computed by its previous iteration $\hat{Y}(m-1)$ after going through the restoration filter \hat{G} and the estimated transfer function \hat{H} . In a first step the image $\hat{Y}(0)$ is equal to the degraded image Y and, after the total number of iterations, the image $\hat{Y}(\bar{m})$ is restored again by the filter \hat{G} leading to the the output image $\hat{X} = \hat{X}(\bar{m})$. This algorithm is somehow based on the same iterative concept of restoration-degradation processes of the MLP but applied to the Fourier domain. Let us recall that the mathematical expressions for this algorithm are particular for each frequency component (ϖ_i, ϖ_j) and, in fact, we put forward that the number of iterations is also a function of these elements, i.e., $\bar{m}(\varpi_i, \varpi_j)$.

It can be easily demonstrated that the filter G' of Fig. 4 is expressed as

$$G' = \hat{G}(\hat{G}\hat{H})^m \quad (24)$$

where $\hat{G}\hat{H}$ is known as the regularization product. In Santiago et al., 2007 we verified that the higher the regularization is, the lower the product $\hat{G}\hat{H}$ becomes with a dynamic range $0 < \hat{G}\hat{H} < 1$.

3.2.1 Sensitivity criteria

So far we have referred to sensitivity as a concept, but now we put it on mathematical expressions. Let us consider that the restoration filter G depends on a set of parameters P_1, P_2, \dots, P_r which can be grouped into the three groups of Section 2.2: blurring, noise and original image. Then we can define the sensitivity S_G regarding the filter G as

$$S_G = \frac{\partial G}{\partial P_1} dP_1 + \frac{\partial G}{\partial P_2} dP_2 + \dots + \frac{\partial G}{\partial P_r} dP_r \quad (25)$$

Analogously, the sensitivity concerning the proposed filter G' can be expressed as follows

$$S_{G'} = \frac{\partial G'}{\partial P_1} dP_1 + \frac{\partial G'}{\partial P_2} dP_2 + \dots + \frac{\partial G'}{\partial P_r} dP_r \quad (26)$$

To compare the sensitivity of both filters we make use of a relative function $Z = S_{G'}/S_G$ which sets the desensitization criteria as $Z < 1$. After differentiating the filter G' of (24) with respect to G we come up with an expression for the relative sensitivity function (see Santiago et al., 2007 for further details)

$$Z(m) = \frac{S_{G'}}{S_G} = (m+1)(\hat{G}\hat{H})^m < 1 \quad (27)$$

As $0 < (\hat{G}\hat{H})^m < \hat{G}\hat{H} < 1$ we can foresee that the function $Z(m)$ of (27) is neither monotonically increasing nor decreasing with the number of iterations m , but it may show a relative maximum extreme depending on the value of the term $\hat{G}\hat{H}$ for a particular pair (ϖ_i, ϖ_j) . This is illustrated in Fig. 5 for several regularization values

Looking into this plot we can observe that the expected maximum extremes of $Z(m)$ depend on the value of $\hat{G}\hat{H}$. The lower the product $\hat{G}\hat{H}$ is, the less iterations m are required to reach the maximum; even high regularization conditions make $Z(m)$ strictly decreasing monotonic. In any case, the main conclusion has to do with the sensitivity condition (27) illustrated by the straight line of the figure. Regardless of the value of the product $\hat{G}\hat{H}$, G' is less sensitive than G if the number of iterations m is high enough. We might therefore increase the value of m as needed to prevent poor restoration results of wrong estimates. However, that is not possible as the restoration error is significantly affected as demonstrated in Santiago et al., 2007.

In González & Woods, 2007 the restoration error is divided into the ringing (or image-dependent) component and the noise-dependent component. What we found out in our

previous analysis is that the trend of both errors is contrary for the desensitized filter G' . Whereas the noise-dependent error is lower as the number of iterations increases, the ringing component gets higher. Consequently, we need to look for a trade-off between the error components while keeping the desensitization criteria true.

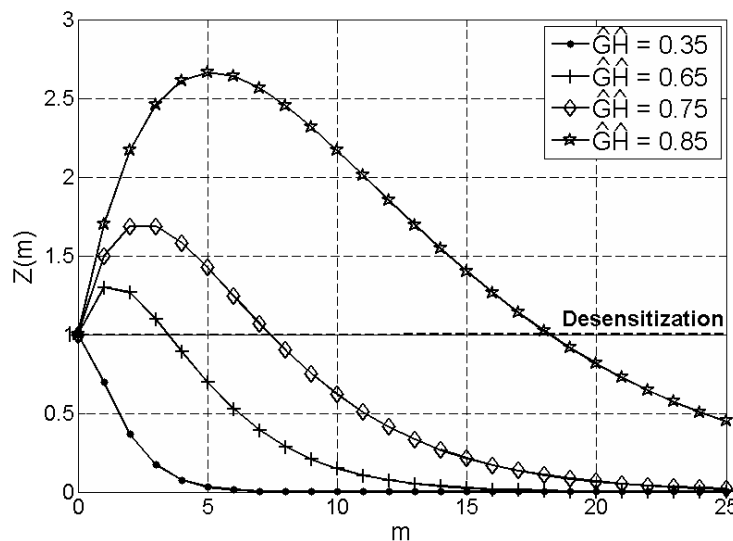


Fig. 5. Relative sensitivity function $Z(m)$.

3.2.2 Number of iterations

Since the relative sensitivity function $Z(m)$ does not have a local minimum as viewed in Fig. 5, let us optimize another $Z(m)$ property which also fulfills the desensitization criteria. In particular, we shall look for a maximum of efficiency for the complexity introduced in the restoration process by increasing the number of iterations from m to $m + 1$. In other words, let us seek a value of m from that on the improvement on desensitization is lower than the incremental complexity. In mathematical terms we can express this efficiency change as the second derivative of $Z(m)$ denoted by $R(m) = Z''(m)$. It can be easily derived from (27) that

$$R(m) = (\hat{G}\hat{H})^m \ln(\hat{G}\hat{H}) [2 + (m + 1)\ln(\hat{G}\hat{H})] \tag{28}$$

The purpose is to maximize this function as well as constrain it to the desensitization condition of $Z(m) < 1$. In Santiago et al., 2007 we came up to a number of iterations as follows

$$\bar{m} = \text{round} \left\{ - \left[1 + \frac{3}{\ln(\hat{G}\hat{H})} \right] \right\} \tag{29}$$

subject to a constraint on the regularization term $0.14 < \hat{G}\hat{H} < 0.84$.

Finally, let us compute some numeric results of the main variables of the desensitization algorithm for different regularization products $\hat{G}\hat{H}$: \bar{m} , $Z(m)$, $\delta_r(m)$ and $\delta_n(m)$, where

these delta functions are respectively the relative error components (ringing and noise) expressed in dB.

$\hat{G}\hat{H}$	\bar{m}	$Z(\bar{m})$	$\delta_r(\bar{m})$	$\delta_n(\bar{m})$
0.20	1	0.40	9.15	-13.98
0.30	1	0.60	8.41	-10.46
0.40	2	0.48	9.43	-15.92
0.50	3	0.50	9.66	-18.06
0.60	5	0.47	9.97	-22.18
0.70	7	0.66	9.94	-21.69
0.80	12	0.89	10.03	-23.26

Table 1. Numeric results for the main functions of the desensitized filter.

Looking at the figures of Table 1 we can see that the improvements achieved for $\delta_n(m)$ are greater than the impairments obtained from $\delta_r(m)$, always satisfying the desensitization condition $Z(m) < 1$. For that reason, we may expect to have good restoration results with a rough estimation of noise in a very wide range, much better than other kind of wrong parameters.

4. Experimental results

In this section we aim to validate the properties of the previous algorithms using a variety of experiments with very well-known 256×256 sized images such as Lena, Barbara or Cameraman, or PSFs widely used in the field as the motion, Gaussian or uniform blurs. Furthermore, we shall compare the results with classic approaches of image restoration to ensure the good performance of our iterative methods.

4.1 MLP experiments

Let us see our problem formulation by means of an example. Fig. 6 depicts the original Barbara image blurred by a motion blur of 15 pixels and 45° of inclination, which turns out a PSF mask of 11×11 in size ($B_1 = B_2 = 5$). We have represented the truncated image \mathbf{y}_{tru} on the right which reflects the zeros at the boundaries and the size of $\tilde{L} = 266 \times 266$. A real model would consist of the $FOV = 246 \times 246$ region of this image which we named as \mathbf{y}_{real} so far. Most recent algorithms deal with this real image but making assumptions about the boundaries and yielding a restored image of 246×246 . Consequently, the boundaries marked with the white broken line on the left are never restored. In contrast, our MLP outcomes a 256×256 sized image $\hat{\mathbf{x}}$ reconstructing the boundary area $B = 251 \times 20$.

To resolve this sort of problems we have implemented the MLP according to the following parameters. In the light of the expression (18) we have used the horizontal and vertical Sobel masks ($N = 3 \times 3$) of Bovik, 2005 for the filters \mathbf{d}^s and \mathbf{d}^v . We already commented that the learning speed of the net is set to $\eta = 2$ and the regularization parameter λ relies on a hand

tuning basis. Regarding the interconnection weights, they do not require any network training so the weigh matrices are all initialized to zero. Finally, we set the stopping criteria as a maximum number of 500 iterations (though never reached) or when the relative difference of the restoration error $E(m)$ falls below a threshold of 10^{-3} in a temporal window of 10 iterations.



Fig. 6. Degraded and truncated image by diagonal motion blur (right) and the expected boundary region to be reconstructed (left).

In order to measure the performance of our algorithm, we compute the standard deviation σ_e of the error image $\mathbf{e} = \hat{\mathbf{x}} - \mathbf{x}$ since it does not depend on the blurred image \mathbf{y} as in the ISNR (Banham and Katsaggelos, 1997). Regarding the boundary reconstruction process we particularize the standard deviation to the pixels of the boundary region B .

4.1.1 Experiment 1

Our first experiment takes the Lena image degraded by several motion and uniform blurs. Regarding the motion blur, we establish 45° of inclination and the length of pixels is varied between 5 and 15. We have used the approximation of Matlab to construct the filter of motion which leads to masks between 5×5 and 11×11 in size. Analogously, the uniform blur is defined with odd sizes between 5×5 and 11×11 . In terms of Gaussian noise we set a ratio of $\text{BSNR} = 20 \text{ dB}$.

The results of the MLP are shown in Table 2. As presumable, the quality of restoration is getting worse as the size of the blur increases, but let us remark that the boundary reconstruction area is also expanding. If we compare the results between blurs we can observe that the uniform mask achieves better values at the boundaries, but lower in the center for the same size. It can be thought of a spatial varying restoration process of the MLP in the center with respect to the boundaries.

To visually assess the performance of the MLP we select some of the results indicated in the previous table. On the left of Fig. 7 we depict the Lena restored image for a diagonal motion blur of 10 pixels. The restored boundary area is 252×16 in size marked by a white broken line and reveals how the borders are successfully regenerated without neither any image

information nor prior assumption on the boundary conditions. Likewise, we illustrate the restored image with a uniform blur of 7×7 on the right and a boundary region of 253×12 .

Motion			
Length	Size	σ_e	$B\sigma_e$
5	5×5	8.70	24.59
6	5×5	8.70	20.58
7	7×7	10.35	27.23
8	7×7	10.25	24.05
9	7×7	10.26	20.96
10	9×9	11.62	26.04
11	9×9	11.50	23.36
12	9×9	11.51	20.85
13	11×11	12.78	25.85
14	11×11	12.61	23.15
15	11×11	12.63	21.10

Uniform		
Size	σ_e	$B\sigma_e$
5×5	8.90	17.29
7×7	11.32	19.64
9×9	13.20	20.64
11×11	14.69	22.27

Table 2. Numeric values of σ_e and $B\sigma_e$ for different sizes of degradation.



Fig. 7. Restored images of the MLP when using motion (left) and uniform (right) blurs.

4.1.2 Experiment 2

This experiment aims to compare the performance of the MLP with other restoration algorithms which need BCs to deal with a realistic capture model: zero, periodic, reflective and anti-reflective as commented in Section 2.1. We have used the RestoreTools, 2007 library patched with the anti-reflective modification which implements the matrix-vector operations for every boundary condition. In particular, we have selected an algorithm of this library named as HyBR (hybrid bidiagonalization regularization) that is a modified version of the Tikhonov regularization.

Let us consider the Barbara image degraded by a 7×7 Gaussian blur and the same additive white noise of the previous experiments with $BSNR = 20$ dB. Fig. 8 shows the restored images of the HyBR method from a real acquisition of $FOV = 250 \times 250$ in size (field of

view). We can observe that the restored images for each boundary condition are all 250×250 sized images which miss the information of the boundaries up to 256×256 . Furthermore, a remarkable boundary ringing can be appreciated for the periodic BCs as result of the discontinuity of the image in the boundaries. As demonstrated in Martinelli et al., 2006 the reflexive and the anti-reflexive conditions perform considerably better removing that boundary effect.

The restored image of our MLP algorithm is shown on the bottom-right of Fig. 8 and makes obvious the good performance of the neural net. First, the boundary ringing is negligible without prior assumption on the boundary condition. Moreover, the visual aspect is better compared to the others which recalls the good properties of the TV regularizer. To numerically contrast the results, the parameter σ_e of the MLP is measured only in the FOV region. It leads to $F\sigma_e = 12.47$ which is notably lower to the values of the HyBR algorithm (e.g. $F\sigma_e = 12.99$ for the reflexive BCs). Finally, the MLP is able to reconstruct the 253×12 sized boundary region and outcomes the original image size of 256×256 .



Fig. 8. Restored images with HyBR under periodic (upper-left), reflective (upper-right) and anti-reflective (bottom-left) BCs. Restored image with our MLP (bottom-right).

4.1.3 Experiment 3

Finally, let us compare with other algorithms of the literature which deal with the boundary problem in a different sense from the typical BCs and that reconstruct the area B bordering the field of view. In recent research Bishop, 2008 proposed a method based on the Bayesian model and treated the truncation effect as modeling error. To make a better comparison we have updated the MLP to leverage the concept of extended image of this method by removing the operator $\text{trunc}\{\cdot\}$ from all formulae of Section 3.1 and setting the observed image \mathbf{y}_{real} at the input of the MLP instead of the truncated image \mathbf{y}_{tru} .



Fig. 9. Restored images with Bishop's method: uniform (upper-left) and Gaussian (bottom-left) blurs. Likewise for MLP: uniform (upper-right) and Gaussian (bottom-right).

Looking at Table 3 we find out that the values of σ_e are quite similar for both methods, being the MLP which outperforms in the Gaussian and motion blurs. But what really deserves attention are the results in the boundary region B . The MLP is considerably better reconstructing the missed boundaries as indicated by the lower values of $B\sigma_e$. Then, it reveals the outstanding properties of the neural net in terms of learning about the unknown image.

Bishop			MLP			
Blur	σ_e	$B\sigma_e$	$F\sigma_e$	σ_e	$B\sigma_e$	$F\sigma_e$
Uniform	13.23	17.43	12.99	13.53	15.05	13.45
Gaussian	12.49	17.79	12.18	12.33	14.13	12.24
Motion	11.37	17.63	10.97	11.33	12.58	11.27

Table 3. Comparison between Bishop's method and MLP for various PSFs

Let us visually assess the performance of both methods for some experiments of Table 3. In particular, we have used two 250×250 sized images degraded by uniform and Gaussian blurs of 7×7 . The restored images appear in Fig. 9 with 256×256 in size and thus reconstructing the boundary area $B = 253 \times 12$. Despite the fact that the value of σ_e is lower for the Bishop's method in the uniform blur, we can observe that the subjective quality of the MLP output is better. As for the Gaussian blur the restored images look similar although the value of σ_e is in favor of the neural net.

4.2 Desensitization experiments

In this case our experiments aim to compare the performance of the desensitization filter G' with respect to the classical filters G Wiener and Tikhonov when having errors on the estimations. So let us define a way to measure the deviations from the real value of the parameters. Let ε_p be the relative error of a generic parameter P defined as follows

$$\varepsilon_p = \frac{P_{real} - P_{estimated}}{P_{real}} \cdot 100 \quad (30)$$

where P_{real} and $P_{estimated}$ stand for the respective real and estimated values of the parameter P . Provided that these parameters are real variables, the relative error ε_p is also extended along the range $-\infty < \varepsilon_p < +\infty$, even though we only consider the significant values ranged between -100 and 100 %.

The types of parameters for these experiments have to do with the noise and blurs of previous experiments. As for the noise we shall deal with the variance σ_n^2 of a Gaussian additive sample (ε_σ). On the other hand, we shall focus on the motion blur so that we can observe the effects of mistaking the angle ϕ (ε_ϕ).

In terms of implementation let us recall that the proposed desensitization algorithm yields a different number of iterations \bar{m} for every pair (ϖ_i, ϖ_j) due to its dependence on the product $\hat{G}\hat{H}$. By using the expression (29) we obtain a value of \bar{m} for those pairs whose regularization term $\hat{G}\hat{H}$ is within the range $0.14 < \hat{G}\hat{H} < 0.84$. Thus, a criterion will be adopted for choosing a number of iterations for the rest of frequencies. Owing to the increasing trend of \bar{m} with respect to $\hat{G}\hat{H}$ (see Table 1), all pairs whose corresponding regularization value exceeds 0.84 are associated to the upper bound of iterations and likewise the minimum value (cero) if $\hat{G}\hat{H}$ is below 0.14.

In view of the expressions (14) and (15) let us do some remarks. First, the spectral density of the Gaussian white noise is just its variance $S_{nn} = \sigma_n^2$. As for the spectral density S_{xx} it is commonly estimated by means of the spectral density of the observed image S_{yy} , which in turn is estimated by the periodogram approximation (Marple, 1987)

$$S_{yy} = \frac{1}{L^2} |Y|^2 \quad (31)$$

Finally, the parameter λ of (15) is typically computed by the discrepancy principle (Bonesky, 2009) which establishes that

$$\|\mathbf{y} - \mathbf{H}\hat{\mathbf{x}}\|_2^2 = \|\mathbf{n}\|_2^2 = L\sigma_n^2 \quad (32)$$

In these experiments we do use the common ISNR (improvements on the signal-to-noise ratio) as the objective metric.

4.2.1 Experiment 1

In a first simulation we shall execute the desensitization filter for the whole range $-100 < \varepsilon_p < +100$ of the relative error of the parameters σ_n^2 and ϕ . The original motion blur is described by a length of 15 pixels and an angle of 45 degrees in a counter-clockwise direction. And the Gaussian noise is added according to a specific BSNR of 20 dB. This experiment is computed for the two original filters Wiener and Tikhonov when facing a degraded image Cameraman.

In Fig. 10 we can observe the regions of desensitization for the Wiener filter. As for the noise estimation the desensitization filter outperforms from a specific value ε_σ on. Regarding the angle estimation ε_ϕ our method achieves better results outside a bandwidth. In Santiago, 2007 it is demonstrated that the desensitization method may completely outperform in case of high enough noise conditions.

If we look into the results of the Tikhonov filter in Fig. 11 we come up with better results as it is required a lower value of ε_σ to be in the desensitization region (with less than 10%). This situation may be typical in a method of estimation of the noise variance and therefore our iterative scheme means a successful solution. With regard to the blur estimation ε_ϕ the region of desensitization is practically the same as in the Wiener example, so it reveals the better behavior of our algorithm in case of the noise.

4.2.2 Experiment 2

Finally, we devote this section to visually analyze the results of the desensitization filter for the optimum case: noise estimation and Tikhonov filter. We shall use the Barbara and Lena images degraded by a Gaussian blur of size 10×10 , and we keep the same noise level as in previous experiments with BSNR = 20 dB. The estimation error ε_σ is fixed to 10%.

We have printed in Fig. 12 the restored images obtained by the Tikhonov and the desensitization filter in each case. It is remarkable how the Tikhonov algorithm is highly

affected by the small error in noise estimation with a significant noise-dependent error on the textures of Barbara and Lena. However, our algorithm is able to counteract this effect and provide a restored image with a better visual aspect. The numeric figures of ISNR also make evidence of this situation. In Barbara we obtain a value of $\text{ISNR} = -2.46$ dB for the Tikhnov filter whereas the desensitization clearly improves it with $\text{ISNR} = 2.38$ dB. Analogously, we end up with $\text{ISNR} = -3.53$ dB and $\text{ISNR} = 2.45$ dB in the Lena example.

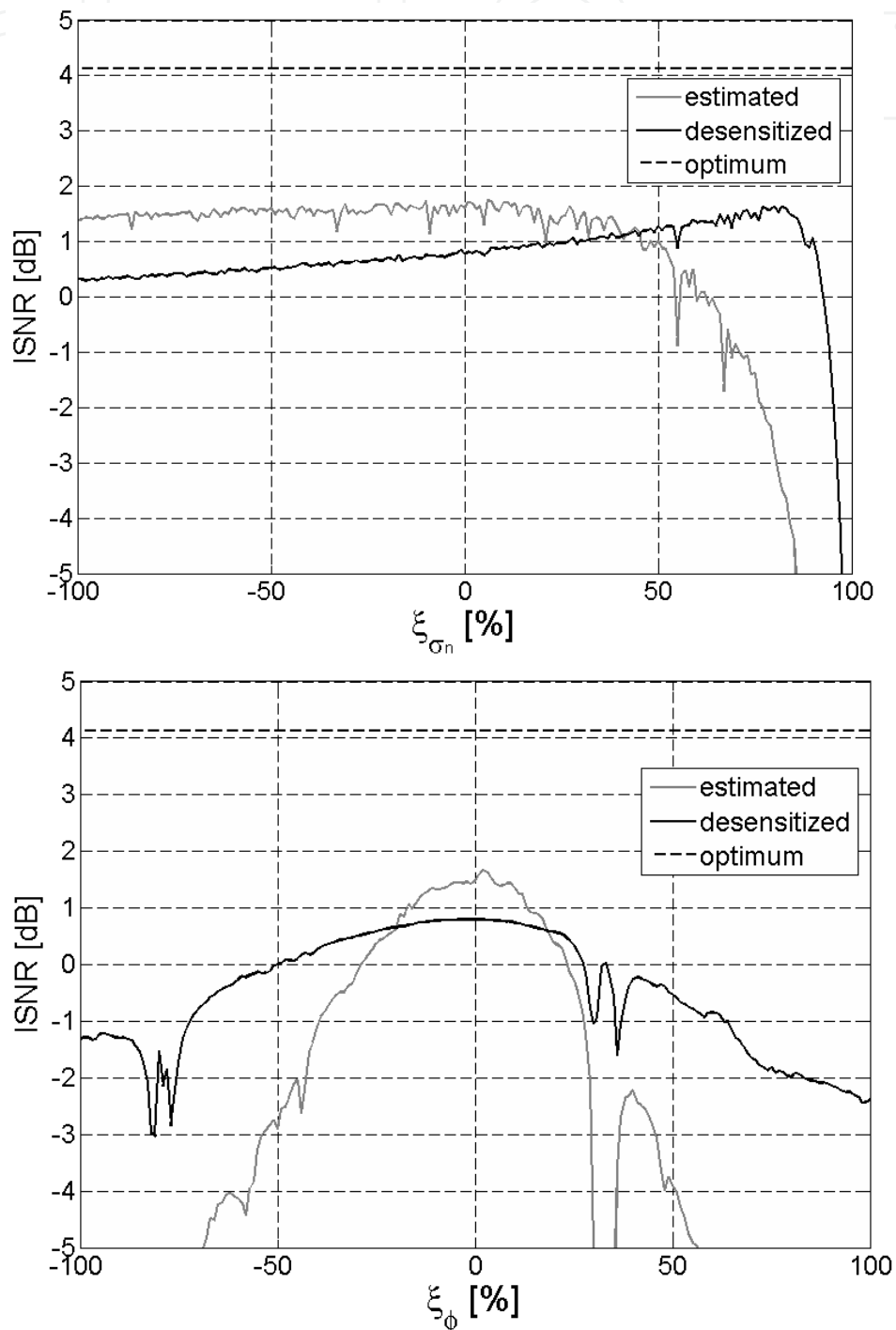


Fig. 10. ISNR for errors on estimations σ_n^2 and ϕ of Wiener filter.

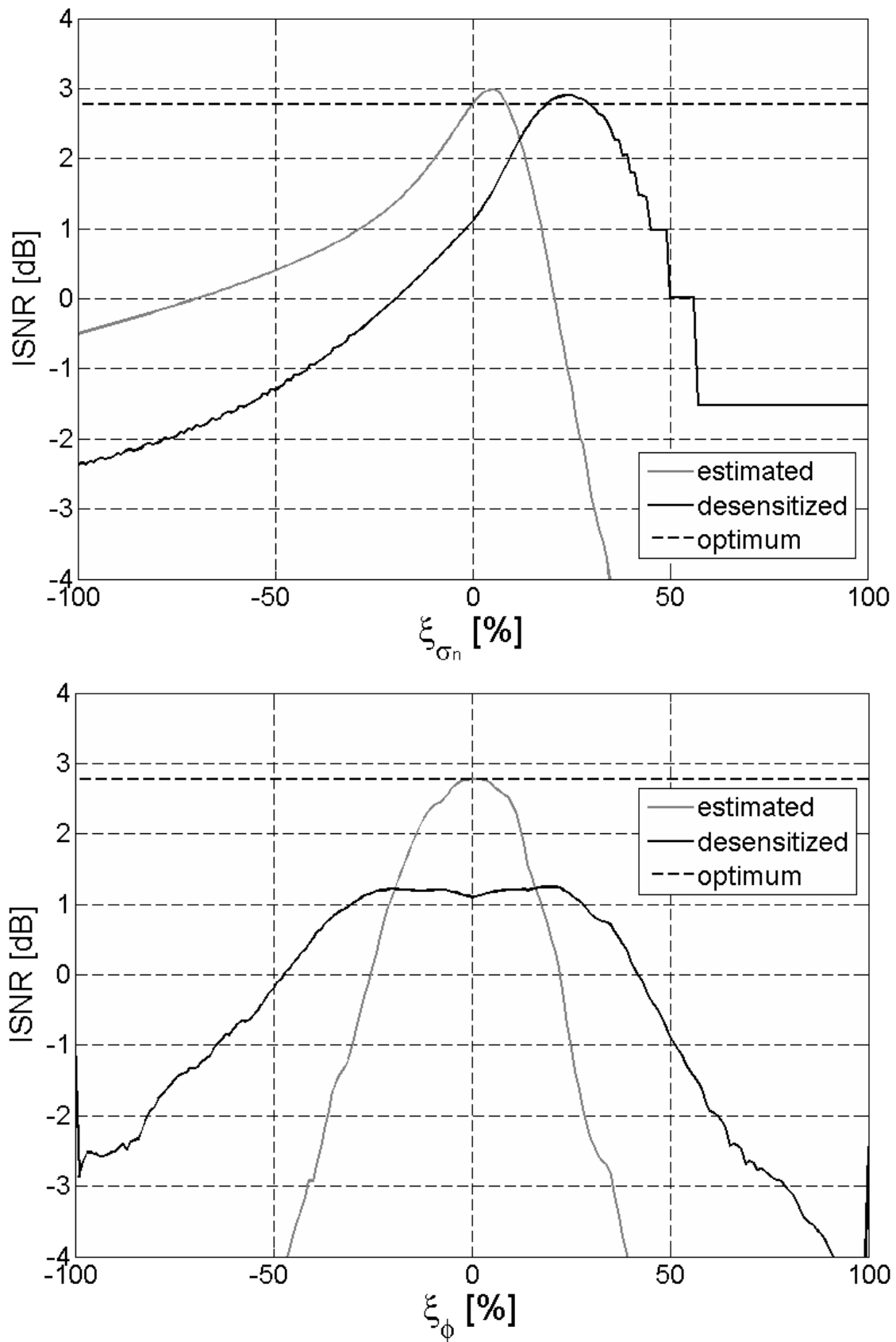


Fig. 11. ISNR for errors on estimations σ_n^2 and ϕ of Tikhonov filter.



Fig. 12. Restored images with Tikhonov filter (upper-left and bottom-left) compared to the restored images of the desensitization filter (upper-right and bottom-right).

5. Conclusion

This chapter has addressed two well-known problems of the regularization solutions in image restoration: dependency of boundary conditions and sensitivity to parameters estimations. Following a similar iterative concept of restoration-degradation we have provided two algorithms in the spatial and frequency domain respectively.

On the one hand, we have presented a neural network which aims to restore a real observed image where the borders outside the field of view (FOV) have been truncated. The idea is to apply a TV-based regularization function in an iterative minimization of a MLP (Multilayer perceptron) according to a backpropagation strategy. It achieves to not only restore the center of the image following the optimum linear solution (the ringing artifact thus being negligible), but also reconstruct the boundary area without any prior.

The proposed restoration scheme has been validated by means of several tests. As a result, we can conclude the ability of our neural net to deal with the non-linearity of border truncation and its learning properties about the degradation model so as to regenerate the missed boundaries. In fact, it clearly outperforms when comparing with other methods of the state-of-the-art which also try to inpaint the boundary area.

The second algorithm of this chapter outcomes a frequency-based restoration filter which desensitizes an original method when having errors on its parameters. By means of an iterative sequence of restoration-degradation processes for each frequency pair we come up with a trade-off between desensitization and restoration error. In particular, the noise-dependent error is more robust to estimations than the ringing error which gets higher as the iterations increase.

Various tests demonstrate that the region of desensitization is located from a low value of parameters errors, being more evident in the noise variance and using the Tikhonov filter. We observed the undesirable effects on the original filter in spite of the low error, while our desensitized filter counteract this noise error with successful results.

6. References

- Banham, M. R. & Katsaggelos, A. K. (1997). Digital Image Restoration. *IEEE Signal Processing Magazine*, Vol. 14, No. 2, pp. 24–41, ISSN 1053-5888
- Bertero, M. & Bocacci, P. (1998). *Introduction to Inverse Problems in Imaging*, Institute of Physics Publishing, ISBN 0750304359
- Bishop, T. E. (2008). *Bayesian image deblurring and boundary effects*, PhD Thesis, University of Edimburg, UK
- Bioucas-Dias, J.; Figueiredo, M. & Oliveira, J. P. (2006). Total variation-based image deconvolution: a majorization–minimization approach, *Proceedings of International Conference on Acoustics, Speech and Signal Processing*, Vol. 2, pp. 861–864, ISBN 1-4244-0469-X, Toulouse, France
- Bonesky, T. (2009). Morozov's discrepancy principle and Tikhonov-type functionals. *Inverse Problems*, Vol. 25, No. 1, Article ID 015015, 11 pages, ISSN 0266-5611
- Bovik, A. (2005). *Handbook of Image & Video Processing* (2nd edition), Elsevier, ISBN 0-12-119792-1, Burlington, USA
- Calvetti, D. & Somersalo, E. (2005). Statistical elimination of boundary artifacts in image deblurring. *Inverse Problems*, Vol. 21, No. 5, pp. 1697–1714, ISSN 0266-5611
- Campisi, P. & Egiazarian, K. (2007). *Blind image deconvolution: theory and applications*, CRC Press, ISBN 0-8493-7367-0, New York, USA
- Chan, T.F. & Shen, J. (2005). *Image Processing and Analysis Variational, PDE, Wavelet and Stochastic Methods*, SIAM, ISBN 0-89871-589-X, Philadelphia, USA
- González, R. C. & Woods, R. E. (2007). *Digital Image Processing* (3rd edition), Prentice Hall, ISBN 0-13-168728-X
- Han, Y. B. & Wu, L. N. (2004). Image restoration using a modified hopfield neural network of continuous state change. *Signal Processing*, Vol. 12, No. 3, pp.431–435, ISSN 1003-0530

- Liu, R. & Jia, J. (2008). Reducing boundary artifacts in image deconvolution, *Proceedings of International Conference on Image Processing*, pp. 505–508, ISBN 978-1-4244-1765-0, San Diego, USA
- Marple, S. L. (1987). *Digital Spectra Analysis: With Applications*, Prentice-Hall, ISBN 0-132-14149-3, Upper Saddle River, USA.
- Martinelli, A.; Donatelli, M.; Estatico, C. & Serra-Capizzano, S. (2006). Improved image deblurring with anti-reflective boundary conditions and re-blurring. *Inverse Problems*, Vol. 22, No. 6, pp. 2035–2053, ISSN 0266-5611
- Molina, R.; Mateos, J. & Katsaggelos, A. K. (1999). Bayesian and regularization methods for hyperparameter estimation in image restoration. *IEEE Transactions on Image Processing*, Vol. 8, No. 2, pp. 231–246
- Molina, R.; Mateos, J. & Katsaggelos, A. K. (2006). Blind deconvolution using a variational approach to parameter, image and blur estimation. *IEEE Transactions on Image Processing*, Vol. 15, No. 12, pp. 3715–3727, ISSN 1057-7149
- Ng, M. K.; Chan, R. H. & Wun-Cheung, T. (1999). A fast algorithm for deblurring models with Neumann boundary conditions. *SIAM Journal on Scientific Computing*, Vol. 21, No. 3, pp. 851–866, ISSN 1064-8275
- Oliveira, J.; Bioucas-Dias, J. & Figueiredo, M. (2009). Adaptive total variation image deblurring: a majorization-minimization approach. *Signal Processing*, Vol. 89, No. 9, pp. 2479–2493, ISSN 0165-1684
- Osher, S.; Rudin, L. & Fatemi, E. (1992). Nonlinear total variation based noise removal algorithms. *Physica D: Nonlinear Phenomena*, Vol. 60, pp. 259–268, ISSN 0167-2789
- Paik, J. K. & Katsaggelos, A. K. (1992). Image restoration using a modified hopfield network. *IEEE Transactions on Image Processing*, Vol. 1, No. 1, pp. 49–63, ISSN 1057-7149
- Restore Tools (2007). In: *Emory University*, 14.10.2011, Available from <http://www.mathcs.emory.edu/~nagy/RestoreTools/>
- Santiago, M. A.; Cisneros, G. & Bernués, E. (2007). Iterative Desensitisation of Image Restoration Filters under Wrong PSF and Noise Estimates. *EURASIP Journal on Advances in Signal Processing*, Vol. 2007, Article ID 72658, 18 pages, ISSN 1687-6172
- Santiago, M. A.; Cisneros, G. & Bernués, E. (2010). An MLP Neural Net with L1 and L2 Regularizers for Real Conditions of Deblurring. *EURASIP Journal on Advances in Signal Processing*, Vol. 2010, Article ID 394615, 18 pages, ISSN 1687-6172
- Sun, Y. (2000). Hopfield neural network based algorithms for image restoration and reconstruction - Part I: algorithms and simulations. *IEEE Transactions on Signal Processing*, Vol. 48, No. 7, pp. 2119–2131, ISSN 1053-587X
- Vogel, C. R. (2002). *Computational methods for inverse problems*, SIAM, ISBN 0-89871-550-4, Philadelphia, USA
- Wang, J.; Liao, X. & Yi, Z. (2005). Image restoration using hopfield neural network based on total variational model, *Proceedings of the Second international conference on Advances in neural networks*, Vol. 2, pp. 735–740, ISBN 3-540-25913-9, Chongqing, China
- Woods, J.; Biemond, J. & Tekalp, A. (1985). Boundary Value Problem in Image Restoration, *Proceedings of International Conference on Acoustics, Speech and Signal Processing*, Vol. 10, pp. 692–695, ISBN 1-4244-0469-X, Tampa, Florida

Wu, Y. D.; Sun, Y.; Zhang, H. Y. & Sun, S. X. (2007). Variational PDE based image restoration using neural network. *IET Image Processing*, Vol. 1, No. 1, pp. 85-93, ISSN 1751-9659

IntechOpen

IntechOpen

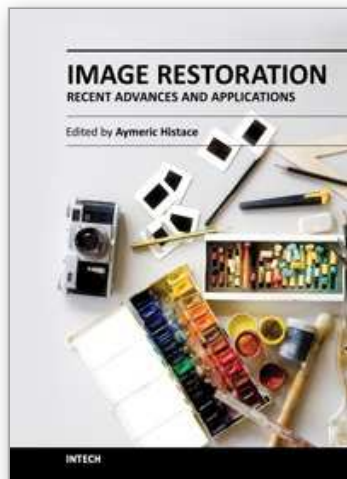


Image Restoration - Recent Advances and Applications

Edited by Dr Aymeric Histace

ISBN 978-953-51-0388-2

Hard cover, 372 pages

Publisher InTech

Published online 04, April, 2012

Published in print edition April, 2012

This book represents a sample of recent contributions of researchers all around the world in the field of image restoration. The book consists of 15 chapters organized in three main sections (Theory, Applications, Interdisciplinarity). Topics cover some different aspects of the theory of image restoration, but this book is also an occasion to highlight some new topics of research related to the emergence of some original imaging devices. From this arise some real challenging problems related to image reconstruction/restoration that open the way to some new fundamental scientific questions closely related with the world we interact with.

How to reference

In order to correctly reference this scholarly work, feel free to copy and paste the following:

Miguel A. Santiago, Guillermo Cisneros and Emiliano Bernués (2012). Iterative Restoration Methods to Loose Estimations Dependency of Regularized Solutions, Image Restoration - Recent Advances and Applications, Dr Aymeric Histace (Ed.), ISBN: 978-953-51-0388-2, InTech, Available from:

<http://www.intechopen.com/books/image-restoration-recent-advances-and-applications/iterative-restoration-methods-to-loose-estimations-dependency-of-regularized-solutions>

INTECH

open science | open minds

InTech Europe

University Campus STeP Ri
Slavka Krautzeka 83/A
51000 Rijeka, Croatia
Phone: +385 (51) 770 447
Fax: +385 (51) 686 166
www.intechopen.com

InTech China

Unit 405, Office Block, Hotel Equatorial Shanghai
No.65, Yan An Road (West), Shanghai, 200040, China
中国上海市延安西路65号上海国际贵都大饭店办公楼405单元
Phone: +86-21-62489820
Fax: +86-21-62489821

© 2012 The Author(s). Licensee IntechOpen. This is an open access article distributed under the terms of the [Creative Commons Attribution 3.0 License](#), which permits unrestricted use, distribution, and reproduction in any medium, provided the original work is properly cited.

IntechOpen

IntechOpen